

Robot-assisted Diagnostic Ultrasound - Design and Feasibility Experiments

S.E. Salcudean, G. Bell, S. Bachmann, W.H. Zhu,
P. Abolmaesumi, and P.D. Lawrence

University of British Columbia
Department of Electrical and Computer Engineering
Vancouver, B.C., Canada, V6T 1Z4
tims@ece.ubc.ca
WWW home page: <http://www.ee.ubc.ca/~tims>

Abstract. Motivated by the need for providing a better user interface for ultrasound technicians, a teleoperation approach to diagnostic ultrasound examinations is proposed in this paper. In this approach, the ultrasound probe is positioned by a robot, with the operator, the robot controller, and an ultrasound image processor having shared control over its motion. An inherently safe, light, backdrivable, counterbalanced robot has been designed for carotid artery examinations. Its design, as well as experiments demonstrating effective free-motion and force control, are presented. The feasibility of using visual servoing for motion in the plane of the ultrasound probe has also been addressed. Using a modified image correlation algorithm, tracking of the carotid artery for periods of time in excess of ten seconds has been demonstrated.

1 Introduction

Medical ultrasound exams often require that ultrasound technicians hold the transducers in awkward positions for prolonged periods of time, sometimes exerting large forces. Not surprisingly, a number of studies indicate that they suffer from an unusually high incidence of musculoskeletal disorders (e.g. [1]).

Motivated initially by the need to alleviate these problems and present a more ergonomic interface to the ultrasound technician, the authors have embarked upon the development of a teleoperation system for medical ultrasound. The system consists of a master hand controller, a slave manipulator carrying the ultrasound probe, and a computer control system that allows the operator to remotely position the ultrasound transducer relative to the patient's body. The problem considered first as a test-bed for robot-assisted ultrasound was that of carotid artery examination. This examination is carried out to detect occlusive disease in the left and right common carotid arteries - a major cause of strokes.

A robot-assisted ultrasound examination system would provide other, not only ergonomic, benefits. For instance, since the location of the ultrasound transducer can be determined via the forward kinematics of the slave manipulator,

three-dimensional ultrasound images can be reconstructed from a series of two-dimensional image slices [4]. Remote probe positioning could also be used in teleradiology. Although a number of methods for transmitting ultrasound images have been proposed in the literature [3], none allow the radiologist to view *and manipulate* the ultrasound transducer at the remote site. The ability to position the ultrasound transducer in response to acquired ultrasound images would also be of benefit to image guided interventions (e.g., percutaneous pericardial puncture) and registration with past examination records or images obtained with other imaging methods (e.g., MRI).

This paper presents significant steps towards a robot-assisted ultrasound examination system. Based on ultrasound transducer position and force measurements taken during carotid artery examinations, a novel fully counterbalanced robot suitable for placing the ultrasound transducer in contact with a patient was designed and is presented in Section 2. The motion of the robot arm and the hand controller of the proposed ultrasound are based on measured positions and forces, acquired ultrasound images, and/or taught position and force trajectories. Several modes of control are discussed in Section 3, including the control of the transducer using ultrasound image tracking, for which the image Jacobian is derived. The feasibility of feature tracking in ultrasound images is discussed in Section 4, where it is shown that a modified correlation method can be used to track the carotid artery over periods of time as long as ten seconds. This will enable users of the system to apply image servoing techniques such as those described in [2], and can be used to follow along an anatomical feature such as a carotid artery, or to keep a feature, such as the tip of a needle, within the image plane.

2 Ultrasound Robot Design

2.1 Measured Motion/Force Requirements

The range of ultrasound probe motions and forces was measured during carotid artery examinations. These involve duplex imaging of the distal end of the common carotid artery and the proximal ends of the internal and external carotid arteries, both longitudinally and transversely, from the clavicle to the mandible on both the left and right sides of the neck.

A 5MHz ultrasound transducer used in the examination was fitted with a JR³ force/torque sensor and the magnetic field sensor of an ATC The BirdTM electro-

magnetic position and orientation sensor, as shown in Fig. 1. The Bird's magnetic field generator was placed near the patient's neck. The ultrasound technician then carried out a carotid artery exami-

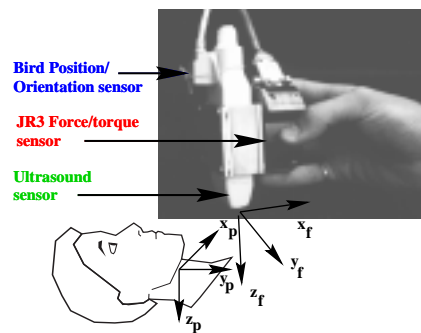


Fig. 1. Apparatus for force-torque-pose experiment

nation on the patient, holding the force/torque sensor instead of the ultrasound transducer (Fig. 1).

Metallic objects in the proximity of magnetic sensors are known to cause significant measurement errors. These were quantified for our experimental setup by placing the instrumented ultrasound transducers in a number of known locations and reading the sensor measurements. An average error of less than 1% was found in orientation, and less than 30% for translation. The measured motion range and the maximum forces encountered are tabulated in Tables 1 and 2. The uncertainty in translational motion range is not of significant concern, as the translational workspace of the robot must be significantly larger than measured in order to comfortably place the ultrasound probe against the patient. The orientation range can be approximated by the right elliptical cone

$$(\tan 15^\circ)^2 x_p^2 + (\tan 35^\circ)^2 y_p^2 = z_p^2, \quad z_p \leq 0, \quad (1)$$

shown, with the measured orientation data, in Fig. 2. Note that the transducer must be able to rotate by $\pm 45^\circ$ about its longitudinal axis everywhere within this right elliptical cone in order to scan transversely and longitudinally.

During these experiments, the maximum velocities recorded, of the order of 0.2 m/s and $260^\circ/\text{s}$, occurred during a switch to a different scanning area or during probe re-orientation. The average velocities were very small, of the order of 5 mm/s and $3^\circ/\text{s}$.

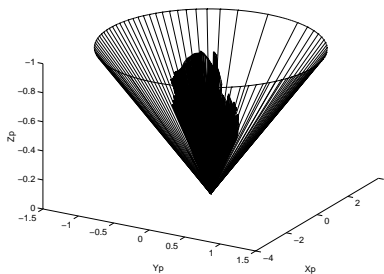


Fig. 2. Orientation range

Translation Range		Angular Range	
Axis	Translation	Axis	Rotation
x_p	130 mm	x_p	35,-50 deg
y_p	150 mm	y_p	-75,75 deg
z_p	100 mm	z_f	-45, +45

Table 1. Probe Motion Estimate

Force Range		Torque Range	
Axis	Force	Axis	Torque
x_f	3.8 N	x_f	0.4 Nm
y_f	4.2 N	y_f	0.7 Nm
z_f	6.4 N	z_f	0.1 Nm

Table 2. Probe Force Estimate

2.2 Robot design

A robot used for ultrasound probe positioning must be safe under any circumstance, including power failure, and should move fast enough to allow the ultrasound examination to take place at a pace close to that achieved by the unassisted sonographer. Therefore, the robot should be light and of limited force ability to allow relatively rapid probe motion in a safe manner. The robot joints should be backdriveable so that the arm could be pushed out of the way if necessary and controlled effectively in force mode. In addition, the robot should cover the required range of motions and forces described above. Because of the large orientation workspace required, the orientation and translation of the probe tip should be approximately decoupled. Otherwise, the entire robot arm has to be moved in order to accommodate probe orientation changes.

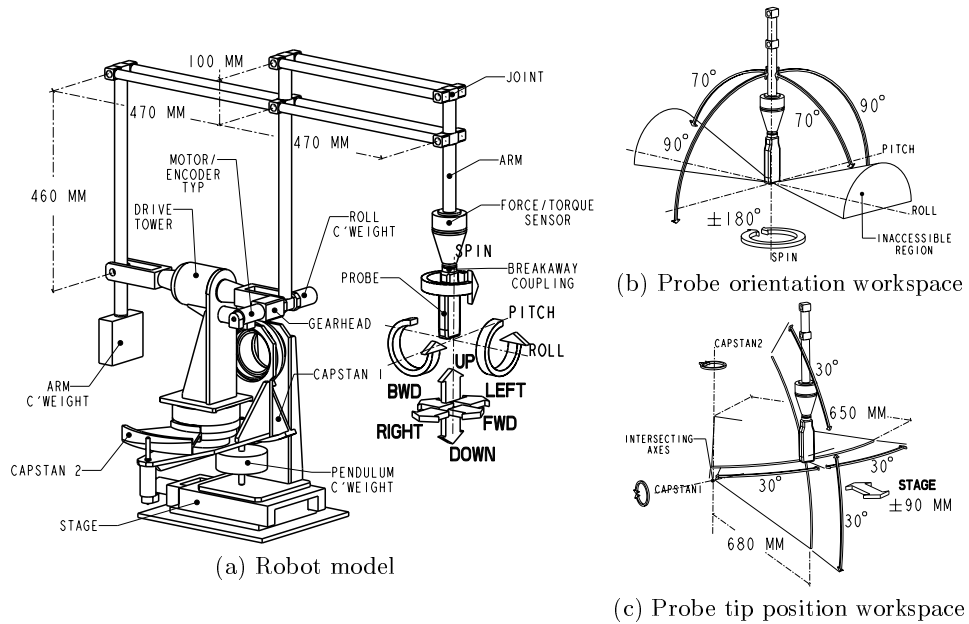


Fig. 3. Ultrasound robot design and workspace

This implies that the arm force capability has to be increased beyond a safe level, or that the arm has to be slowed down beyond an acceptable performance level. A number of design options, such as the use of a spherical wrist, were eliminated by testing whether the range of orientations in the elliptical cone (1) could be attained without interference and with reasonable link lengths. The only remote-center wrist structure that was found to satisfy the orientation range requirement was a rotating parallelogram linkage as used in the LARS robot [5]. The parallelogram linkage used in our design differs because of the need to counterbalance the arm.

The solid model of the robot is shown in Fig. 3, and a photograph is shown in Fig. 4. The robot is placed at the head of the bed, with the labeled LEFT, FWD and DOWN directions coinciding with the x_p , y_p , and z_p axes of Fig. 1, respectively.

The robot supports a probe at the distal end of a lightweight, stiff arm that provides clearance for the patient's head. The probe is mounted on a breakaway magnetic coupling and its spin motor is housed in a cone that attaches to a JR³ force/torque sensor. A rigid drive tower with an offset motor rolls the parallelogram linkage. Two capstan drives with intersecting axes move the probe up-down and left-right, and are mounted on a low friction (<0.007 N-m) linear



Fig. 4. Photograph of the ultrasound robot

stage that can move the probe along the neck of the patient. Each capstan is mounted on a single crossed-roller bearing, and each uses 1 mm diameter coated, annealed, steel cable, pre-loaded with a tensioning device.

Capstan drives were chosen over translational stages to maximize the workspace and minimize the inertia seen at the probe. Note that most of the time, the parallelogram linkage is rolled to one side or the other, and therefore most of the probe normal force is controlled by capstan 2,

Axis	Trans. ratio	Motor	Force/Torque @ Current
Roll	93.6:1	Maxon 90	12.28 N m @ 2.5A
Pitch	50:1	Maxon 90	6.56 N m @ 2.5A
Capstans	40:1	Maxon 90	10.50 N m @ 5A
Spin	1:1	Maxon 20	0.18 N m @ 5A
Stage	0.49 $\frac{\text{rad}}{\text{mm}}$	Maxon 90	15 N* @ 2.5A
Probe Force			10-15 N**

* software limited ** configuration dependent

Table 3. Actuation system characteristics

which has the least mass and therefore allows for higher bandwidth force-control.

The parallelogram linkage was constructed with carbon-fiber tubes and magnesium joints (the arm itself weighs less than 2.4kg including the ultrasound probe and its spin motor). Three adjustable counterweights were used to fully balance the robot. The roll and arm counterweights place the center of mass of the parallelogram linkage at a fixed point on the linkage roll axis, independently of the ultrasound transducer orientation. Because of mechanical interference (e.g. between the arm counterweight and the capstan), the roll axis had to be placed above capstan 1, creating an unstable inverted pendulum with the center of mass above the capstan 1 axis. This center of mass of this pendulum was moved below the capstan 1 axis by a pendulum counterweight.

As seen in Fig. 3 (b),(c), the ultrasound transducer workspace exceeds the specified requirements significantly.

3 Teleoperation and Shared Control

A signal flow diagram and the present hardware implementation for the teleoperation system are illustrated in Fig. 5. During the ultrasound examination, the operator controls the ultrasound machine as usual, but moves a hand-controller or joystick instead of the ultrasound probe.

During the ultrasound examination, the operator controls the ultrasound machine as usual, but moves a hand-controller or joystick instead of the ultrasound probe. Some of control modes that have been tested or are envisaged are: **Master-slave mode without force feedback**, with the ultrasound transducer tracking a linear combination of force and velocity of the joystick command. A Logitech Magellan [6] has been used as a joystick in this mode and experimental results are described below.

Master-slave mode with force feedback, as described in [8], using the hand-controller described in [7]. Feasibility experiments have been carried out [8].

Shared operator/robot controller mode, in which the two modes specified

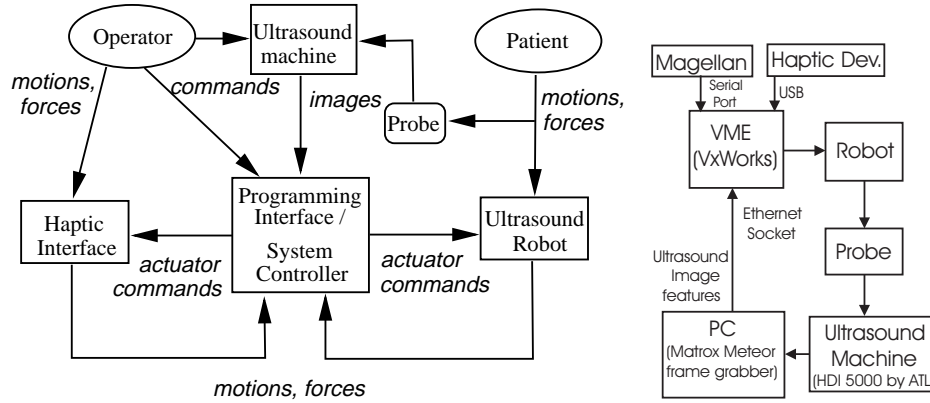


Fig. 5. Signal flow and present hardware implementation for the teleoperation system

above might be used along some of the degrees of freedom, but not others. For example, the probe force along its beam center axis z_f could be controlled or kept within safe pre-specified values by the robot controller.

Shared operator/robot controller/image processor control, in which visual servoing can be used to control up to three degrees of freedom - the translation and rotation of the ultrasound transducer in the plane of the ultrasound beam, while the operator and robot controller control the other degrees of freedom. The image Jacobian obtained below demonstrates that indeed the three degrees of freedom in the ultrasound image plane are controllable, while the ability to track features in ultrasound images over tens of seconds with a modified image correlation technique has also been demonstrated and is summarized in Section 4.

3.1 Force/velocity control

Because the robot is counterbalanced and velocities are small, the robot dynamics simplify to

$$M(\theta) \cdot \ddot{\theta} = \tau - J^T \cdot F \quad (2)$$

where $\theta \in R^6$ denotes the robot joint variables, $M(\theta) \in R^{6 \times 6}$ is the joint space mass matrix, $\tau \in R^6$ denotes the control torques, $J \in R^{6 \times 6}$ is the Jacobian matrix, and $F \in R^6$ is the force/moment exerted on the patient.

The control approach is illustrated in Fig. 6. Its objective is to let a linear combination of the ultrasound probe velocity and scaled force track the Magellan joystick command (displacement), i.e.

$$\dot{X} + K_f \cdot F = \text{Command}, \quad (3)$$

where $\dot{X} \in R^6$ denotes the linear/angular velocity of the end-effector and K_f is a force scaling matrix. When in free motion where $F = 0$, the ultrasound transducer Cartesian velocity tracks the command; while in contact motion where

\dot{X} is very small, the contact force is controlled by the command proportionally. There is no explicit switching between the contact and free motion states.

The joint space control law in Fig. 6 is designed as

$$\tau = M(\theta) \cdot [\ddot{\theta}_d + \lambda \cdot \dot{e}] + K_s \cdot S + K_I \cdot S^* \quad (4)$$

$$\ddot{\theta}_d = C \cdot (\dot{\theta}_d^* - \dot{\theta}_d) \quad (5)$$

$$S = \dot{e} + \lambda \cdot (e + \zeta) \quad (6)$$

$$\dot{S}_i^* = \begin{cases} S_i \frac{\underline{S}_i^*}{S_i} \leq S_i^* \leq \overline{S}_i^* \\ 0 & \text{otherwise} \end{cases} \quad (7)$$

$$\zeta_i = \begin{cases} \delta_i - e_i, & e_i > \delta_i \\ -\delta_i - e_i, & e_i < -\delta_i \\ \zeta_i & \text{otherwise} \end{cases} \quad (8)$$

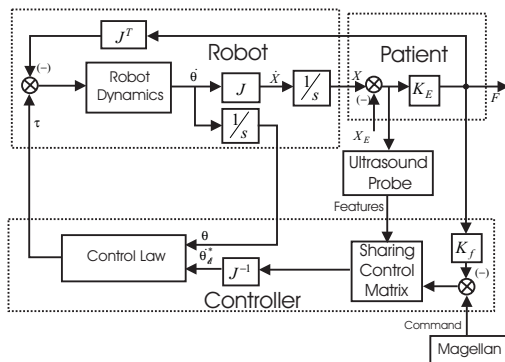


Fig. 6. Velocity/force control

where $e = \theta_d - \theta$, the subscript i denotes the i^{th} entry of a vector,

$\lambda > 0$ is a control parameter determining the compliance of the arm, δ is a vector of small positive threshold elements, and K_s and K_I are two positive-definite gain matrices. C is a filter parameter, and S^* is an integral term with lower and upper bounds \underline{S}^* and \overline{S}^* , respectively.

The control law (4) implements a joint-space PID controller with saturated integral terms and mass and acceleration feedforward, modified by a “reset” function ζ defined in (8) that never allows position errors to be large. Under normal operation, absolute joint position errors will be limited by δ_i , i.e. $|(e + \zeta)_i| \leq \delta_i$. Should the patient or the ultrasound technician attempt to push the robot out of the way, ζ becomes active in such a way that the absolute position errors are still bounded by δ . Should the robot return to normal operation, it will stay close to where it was released, with an error determined by the size of δ . Note that the reset function does not require force sensor input. The natural low stiffness of the arm allows it to be moved away by pushing on any part of the arm linkage. The proportional and integral control terms are not allowed to increase, and therefore wind-up effects (the robot swinging when the patient’s push subsides) do not exist.

The contact force F is handled in two ways. First, it is treated as a disturbance in the robot dynamics and is compensated by S^* . Second, F is measured by the force sensor and is used to achieve the control objective (3).

3.2 Visual Servoing and Feature Tracking

Visual servo-control [2] could be used to control motion in the plane of the ultrasound beam. Its feasibility can be determined by examining the ultrasound image Jacobian J_v , which relates differential changes in image features to differential changes in the configuration of the robot [2]. Let p_i be a feature point in the plane of the ultrasound beam with coordinates $[^f x_i, ^f y_i, ^f z_i]^T$ in the

probe-attached frame. Assuming an orthographic projection model with scale a for the ultrasound image and that p_i remains in the image plane, the coordinates of p_i in the two-dimensional ultrasound image become $[0, u_i, v_i]^T = [0, a^f y_i, a^f z_i]^T$. It can be shown that

$$\begin{bmatrix} \dot{u}_i \\ \dot{v}_i \end{bmatrix} = \begin{bmatrix} 0 & -a & 0 & v_i & 0 & 0 \\ 0 & 0 & -a & -u_i & 0 & 0 \end{bmatrix} {}^f \dot{X} = J_{v_i} {}^f \dot{X} \quad (9)$$

where ${}^f \dot{X}$ are the translational and angular end-effector velocities in end-effector coordinates. If several points are considered in the image, similar pairs of rows will be added to (9). The rank of the resulting Jacobian is at most three. Two or more feature points non-colinear with the origin will generate a Jacobian of rank three. Thus, as expected, with non-trivial ultrasound images, it is possible to control the motion of the ultrasound transducer in its image plane.

4 Experimental Results

4.1 Teleoperation Control

The control approach proposed in Section 3.1 was implemented with the hardware described in Fig. 5. Figs. 7 and 8 demonstrate its effectiveness. The operator controls the robot in vertical motion. Scaling parameters were set such that the maximum 1.5 mm Magellan joystick motion corresponds to a transducer velocity of 0.18 m/s and a force of 36 N. Actual forces are limited to 20 N by the robot capability and to 10 N by software and hardware. Free motion with velocity tracking is displayed until approximately $t = 10s$, when the probe contacts a person's forearm until $t = 30s$.

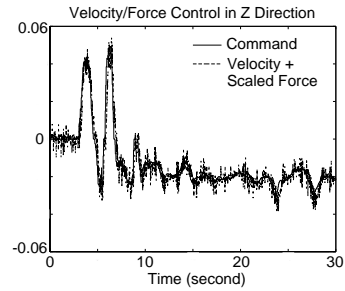


Fig. 7. Tracking of velocity plus scaled force *vs* command in the z_p direction

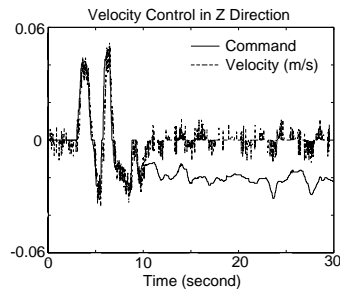


Fig. 8. Velocity tracking

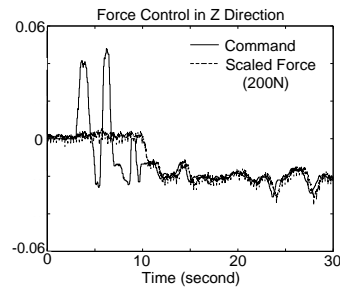


Fig. 9. Force tracking

Fig. 7 illustrates the excellent tracking between the command and the linear combination of velocity and scaled force. Fig. 8 shows excellent velocity tracking in free motion, but not in contact motion. Fig. 9 demonstrates excellent tracking of scaled force in contact motion. It is clear that the both position and forces are followed precisely with appropriate switching between free motion and contact.

Some of the safety features built into the controller and robot design were also successfully tested. The robot could be easily moved away with a single hand, and would remain put in the position in which it was left by the operator. Turning the motor current drivers off left the robot in equilibrium.

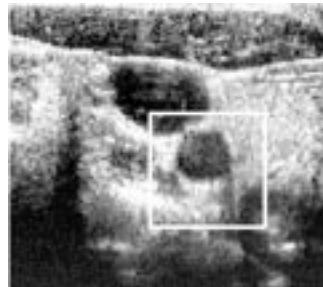
4.2 Feature Tracking in Ultrasound Images

Motion tracking of a region of interest in B-mode ultrasound images was demonstrated before (see, e.g., [9]), but with different goals. Of particular interest to the problem of visual servoing and shared control is the ability to track images over a long period of time. A normalized cross-correlation technique was modified for this purpose and is presented here.

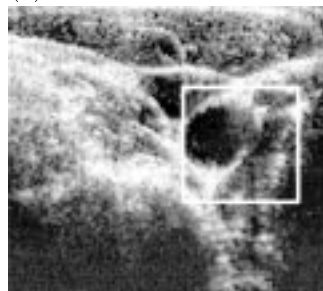
Video-images from an ultrasound examination were obtained. Typical transverse scans clearly showing the carotid artery are shown in Fig. 10. The video images were digitized and processed using a 233 MHz Pentium II PC with a Matrox Meteor frame-grabber.

In a normalized cross-correlation technique, a sub-block of the image (in this case, a 128×128 pixel area containing the carotid artery) acquired at time t_i is shifted in its vicinity looking for a best correlated match with a fixed sub-block of the same size in a prior frame t_k . If k is fixed, the best correlation is sought relative to a fixed or reference image. Applying the cross-correlation method in this way leads to little drift, but high sensitivity to image deformation. If $i - k$ is fixed, the best correlation is sought relative to an image acquired a fixed time offset relative to the current frame. Applying the cross-correlation method in this way leads to little sensitivity to image deformation, but to significant drift, as the shift estimate is being integrated. A mixed approach was implemented that seeks the best correlation relative to multiple frames at times $t_k, t_{k-2}, t_{k-4}, \dots, t_{k-2^n}$, where n is fixed.

Assuming only translational displacements, image sub-blocks of 128×128 of the carotid artery could be tracked at 30 frames/second most often in the range of 5 to 10 seconds, and for as long as 30 seconds.



(a) Initial image.



(b) Final image.

Fig. 10. Images of the carotid artery taken ten seconds apart.

5 Conclusions

A robot-assisted system for performing ultrasound examinations was proposed in this paper with the goal of providing a more ergonomic interface for sonographers. A prototype problem, that of carotid artery examination, was considered. A novel safe robot with large workspace was designed and built and its control in velocity/force mode was demonstrated. The feasibility of tracking ultrasound image blocks over significant time intervals was also demonstrated. In the immediate future, the system will be used to explore the use of operator-computer shared control of the ultrasound probe and ultrasound image servoing. It is hoped that other applications of the system, including the ability to acquire 3-D images and to perform precise registration will also be developed.

6 Acknowledgments

Discussions with Prof. David Lowe and Dr. Paul Trepanier, help with imaging from Henry Wong, machining and robot construction by David Fletcher and Peter Vautour are gratefully acknowledged. This work is supported by the Canadian IRIS Network of Centres of Excellence project SAL.

References

1. H. E. Vanderpool, E. A. Friis, B. S. Smith, and K. L. Harms, "Prevalence of carpal tunnel syndrome and other work-related musculoskeletal problems in cardiac sonographers," *Journal of Occupational Medicine*, vol. 35, pp. 604-610, June 1993.
2. P. I. Corke, *Visual Control of Robots: High Performance Visual Servoing*, John Wiley & Sons Inc., 1996.
3. J. W. Sublett, B. J. Dempsey, and A. C. Weaver. Design and implementation of a digital teleultrasound system for real-time remote diagnosis. In Proceedings of the 1995 Symposium on Computer-Based Medical Systems, pages 292-298, 1995.
4. J. F. Brinkley, W. E. Moritz, and D. W. Baker. Ultrasonic three-dimensional imaging and volume from a series of arbitrary sector scans. *Ultrasound in Medicine and Biology*, 4:317-327, 1978.
5. R. H. Taylor, J. Funda, B. Eldridge, S. Gomory, K. Gruben, D. LaRose, M. Talamini, L. Kavoussi, and J. Anderson. A telerobotic assistant for laparoscopic surgery. *IEEE Engineering in Medicine and Biology Magazine*, 14(3):279-288, May/June 1995.
6. Hirzinger, G., Dietrich, J., Gombert, B., Heindl, J., Landzettel, K., Schott, J., "The sensory and telerobotic aspects of the space robot experiment ROTEX," in *Int. Symp. on Artificial Intel., Rob. and Aut. in Space*, (Toulouse, France), Sept. 30-Oct. 2, 1992.
7. S.E. Salcudean and N.R. Parker, "6-DOF Desk-Top Voice-Coil Joystick", *Symp. Haptic Interfaces for Virtual Env. and Teleop. Syst., Intl. Mech. Eng. Congr. Exp.*, DSC-Vol. 61, pp. 131-138, Dallas, Texas, Nov. 16-21, 1997.
8. W.H. Zhu and S.E. Salcudean, "Teleoperation with Adaptive Motion/Force Control", to appear in the 1999 *IEEE Intl. Conf. Rob. Aut.*, Detroit, USA, May 1999.
9. E.J. Chen, I.A. Hein, J.B. Fowles, R.S. Adler, P.L. Carson, and W.D. O'Brien Jr., "A Comparison of the Motion Tracking of 2-D Ultrasonic B-Mode Tissue Images with a Calibrated Phantom", 1991 *IEEE Ultrasonic Symposium*, pp. 1211-1213.